Atomization and Sprays, 23 (4): 297–325 (2013)

LARGE EDDY SIMULATION OF HIGH GAS DENSITY EFFECTS IN FUEL SPRAYS

O. Kaario,[1,*] V. Vuorinen,[1] T. Hulkkonen,[1] K. Keskinen,[1] M. Nuutinen,[1] M. Larmi,[1] & F. X. Tanner[2]

[1]*Aalto University School of Engineering, P.O. Box 14300, FIN-00076, Aalto, Finland*

[2]*Michigan Technological University, MI 49931-1295, USA*

[*]Address all correspondence to O. Kaario E-mail: ossi.kaario@aalto.fi

Original Manuscript Submitted: 14/12/2012; Final Draft Received: 18/06/2013

The paper focuses on the physics of sprays using large eddy simulation (LES) and Lagrangian particle tracking (LPT). The LES/LPT was compared to previously unpublished experimental fuel spray data in two ambient gas densities, 39 and 115 kg/m^3. The higher density case corresponds to a near-future engine environment with maximum cylinder pressure of the order of 300 bar, whereas the lower density case resembles typical present-day engine conditions. The accuracy of the results was quantified by calculating the resolved part of the turbulent kinetic energy and using a LES quality index analysis. The sprays produced by the LES/LPT had many similarities with the experimental sprays. On a global scale, spray penetration, spray opening angle, and spray dispersion were found to be well captured by the LES/LPT. The results indicated that the effect of subgrid scales on particle dispersion was small and hence no explicit particle dispersion model was required. Similarities were also found locally as LES/LPT produced small-scale flow structures indicated by the Q-criterion, preferential concentrations, and voids free of droplets. Finally, we propose a new gas phase mixing indicator in order to quantify turbulent mixing. Results from the novel mixing indicator suggest that for a given spray penetration, the higher ambient gas density spray yields an increased mixing rate.

KEY WORDS: *large eddy simulation, fuel spray, gas density, gas mixing*

1. INTRODUCTION

The demand for specific power from engines is continuously increasing as the trend in engine development is towards smaller-size engines. One effective way to augment engine power is to increase maximum cylinder pressure. By raising pressure, gas density also increases. However, it is widely established that gas density has a significant effect on fuel spray behavior in engines. Typically, when considering global spray parameters, as gas density increases, the spray tip penetration decreases and the opening angle increases (Naber and Siebers, 1996). As a consequence, the fuel vapor mixing behavior and the subsequent combustion and emission formation processes are affected by the

change in the gas density. In diesel engines, the main emissions of concern are soot and NO_x, which are strongly influenced by mixture quality inside the fuel spray (Stiesch, 2003). Thus, various studies have addressed the spray formation problem from both experimental and computational viewpoints (Crowe et al., 1998; Eaton and Fessler, 1994; Elghobashi, 1991, 1994; Faeth, 1996; Luo et al., 2006). Currently, there are research engines already operating at the 300 bar cylinder pressure level, indicating average gas densities of more than 100 kg/m^3 (Kaario et al., 2010a,b). This necessitates the investigation of the mixing characteristics of fuel sprays injected into high gas density atmosphere.

When discussing mixing in the context of sprays, the effect of droplets on the carrier phase enters in the form of the time it takes for the droplet to adjust to the local flow conditions. This is characterized by the Stokes number $\mathrm{St} = \tau_p/\tau_f$, where τ_f is the flow time scale and τ_p is the droplet time scale written as $\tau_p = \rho_p d^2/18\rho_g\nu_g$, where ρ_p is the droplet density, d is the droplet diameter, ρ_g is the gas density, and ν_g is the kinematic viscosity. Consequently, the Stokes number definition reveals that an increase in gas density decreases the St number as $\mathrm{St} \sim 1/\rho_g$. This implies that an increase in gas density enhances droplet mixing. An additional view on the effect of gas density is obtained when looking at the readiness of a droplet to break up due to aerodynamic forces according to the Weber number $\mathrm{We} = \rho_g {U_p}^2 d/\sigma$, where U_p is the droplet relative velocity and σ is the surface tension. This shows that an increase in gas density leads to a higher We number indicating a faster breakup process. Furthermore, a characterization of the state of the flow is obtained from the Reynolds number written for the spray induced gas jet as $\mathrm{Re} = \rho_g U D/\mu_g$, where μ_g is the dynamic viscosity and D is the jet diameter. Evidently, an increase in gas density leads to an increase in the Re number, suggesting that the flow becomes more turbulent and thereby increased mixing should be expected. On the basis of the effects from increased gas density, it can be concluded that the mixing is expected to increase and smaller droplets are expected to form, which will follow the turbulent flow field more closely.

Previous studies have implied (Apte et al., 2003a; Oefelein et al., 2007; Vuorinen et al., 2010a) that the boundary condition applied in the near-nozzle region should be carefully considered. When a high-pressure fuel spray emerges from a nozzle hole, there is typically an intact liquid core of a characteristic length. The exact length of the liquid core has been under discussion for a long time mainly because of the difficulties in measuring the high density near nozzle region. However, recent advances in experimental and numerical methodologies have given more insight into the topic. Namely, the current view is that the intact liquid core length is assumed to be relatively short, probably only a few nozzle hole diameters (Smallwood and Glder, 2000; Yeh et al., 1995; Lai et al., 1998; Parker et al., 1998). Additionally, for example Hillamo et al. (2010), Chesnel et al. (2011), and Demoulin et al. (2012) found interaction of turbulent flow structures and small droplets only a few millimeters from the nozzle exit indicating very fast atomization and also suggesting short liquid core length. Furthermore, considering the intact liquid core length within varying ambient density, correlations of the form

$L_c/d \sim (\rho_p/\rho_g)^{1/2}$ have been proposed by several authors (Hiroyasu and Kadota, 1974; Chehroudi et al., 1985; Faeth, 1996). This implies that an increasing ambient density shortens the intact liquid core.

In a fuel spray with some typical fuel amount, there are of the order of $\sim 10^9$ droplets during the fuel injection process (assuming a droplet size of 2 μm). Computing the trajectory of each droplet might be too time-consuming and hence groups of droplets are tracked instead. This is the so-called parcel method, in which the motion of parcels is tracked. Each of the parcels contains a given number of physical particles/droplets that all have the same properties. However, there is an inherent problem in Lagrangian particle tracking (LPT) with very fine grids because a basic assumption in LPT is that droplets are non-displacing, which requires that the volume of a droplet is smaller than that of a computational cell volume (Stiesch, 2003). Therefore, in the present study, simulations are initiated some distance from the injector at $z \sim 6d_n$ to avoid the very dense liquid core region near the injector (Fig. 1). On the other hand, problems may also arise if the computational mesh is too coarse so that a large part of the turbulent energy is not resolved but modeled by the subgrid-scale model. This may lead to too low turbulence production at the near nozzle region and underestimation of slip velocity. A possible remedy for this is to increase the turbulent viscosity explicitly (Gong, 2012) or by introducing an additional source term from droplets to the carrier phase (Bharadwaj and Rutland, 2010). The drawback of these approaches is that the large eddy simulation (LES) sprays may start to resemble Reynolds-averaged Navier–Stokes (RANS) sprays due to the increased viscosity. Consequently, it is important to select proper mesh density for LES/LPT spray simulations as shown for example by Hori et al. (2006). High-fidelity LES studies have been performed in the context of sprays using LPT methodology revealing the fact that when applied correctly, LES/LPT can reproduce the experimentally observed transient flow characteristics (Apte et al., 2003a,b; Oefelein et al., 2007; Vuorinen et al., 2010a,b, 2011).

The objectives of the present study are to (1) compare the results produced by the developed LES/LPT model to previously unpublished experimental fuel spray data, (2)

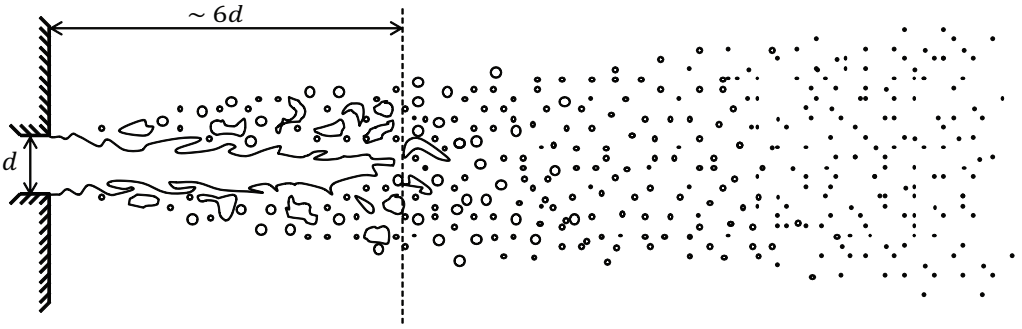

FIG. 1: Schematical representation of the starting location of the modeling at $z \sim 6d_n$.

quantify the effects of ambient gas density variation between 39 and 115 kg/m^3 on fuel sprays, (3) analyze the accuracy of the LES/LPT model by several methods, and (4) develop and apply a new gas phase mixing indicator to reveal differences in mixing due to gas phase density effects. These topics will be carefully considered in the following sections.

2. NUMERICAL MODELING

2.1 Computational Setup and Boundary Conditions

The computational mesh is shown in Fig. 2. The domain length in the streamwise direction is $98D$ (z-direction) and in the transverse directions it is $78D$ (x- and y-directions). The jet diameter D depends on the nozzle hole diameter as $D = 3d_n$ and is either 1.11 or 1.02 mm in the 39 and 115 kg/m^3 gas density cases, respectively. A uniform Cartesian mesh with $\triangle x = \triangle y = \triangle z = 125$ μm is used in the densest part of the computational domain covering most of the spray volume during the injection time. The dense part of the mesh is $59D$ in the streamwise and $16D$ in the transverse directions. The mesh is fully constructed of hexahedral cells without mesh stretching, allowing better numerical accuracy and also avoiding the singularity typically associated with polar meshes. The mesh resolution close to the jet exit is smaller than $D/8$. According to (Pope, 2001; Celik et al., 2005), about 80% of the turbulent kinetic energy can be resolved with the used resolution, and as such the mesh density can be considered to be adequate. The mesh contains about 8 million cells. The walls of the computational domain are adiabatic with a no-slip condition applied for velocity. They have been set relatively far away from the injector axis to reduce possible effects between the spray and the walls. The outer dimensions of the mesh are 80 mm in the x- and y-directions, and 100 mm in the z-direction.

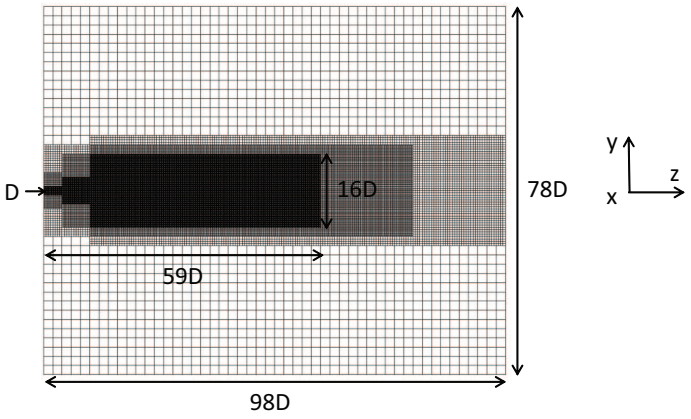

FIG. 2: Computational domain. The dimensions of the mesh are 80 mm in the x- and y-directions, and 100 mm in the z-direction.

The non-dimensional total injection time is $120T$ and $160T$ in the 39 and 115 kg/m^3 gas density cases, respectively, or $\tau_{inj} = 1.7$ ms, where the integral time scale is defined as $T = D/U$. The time step size in the present study is $dt = 5 \times 10^{-7}$ s. The Reynolds number of the spray induced gaseous jet at the droplet origin is $\mathrm{Re} = \rho_g UD/\mu_g$ = 170,000 and 650,000 in the 39 and 115 kg/m^3 gas density cases, respectively, indicating more turbulent conditions in the higher gas density case. The main reason for the higher Re number in the 115 kg/m^3 gas density case is in the higher gas density ut also in the somewhat higher gas jet velocity (due to boundary condition given in Fig. 3). Furthermore, in the present study, a constant value is used for the gas phase viscosity $\mu_g = 1.8 \times 10^{-5}$ kg/ms. However, the temperature variation is commonly taken into account using the Sutherland formulation (Vuorinen et al., 2013). Additionally, when gas pressure increases, the gas viscosity also increases. This effect is, however, rather modest for air (Lemmon and Jacobsen, 2004) for the non-combusting conditions used in the present study (gas pressure in the 39 kg/m^3 case is 34 bar and gas pressure in the 115 kg/m^3 is 98 bar). The increase of gas viscosity in the higher density case can be estimated to be about 10% or less compared to atmospheric pressure. In the present LES/LPT, however, the turbulent viscosity can be $\sim$700 times higher than the dynamic gas viscosity (close to the nozzle). Thereby, the effect of the increased dynamic gas viscosity due to the higher gas pressure can be considered to be negligible. The spray-induced gas jet velocity at the droplet origin is perturbed with uniformly distributed random noise where the amplitude of the fluctuations given is 5% from the gas jet velocity.

The liquid fuel mass flow rates and injection velocities at the jet exit are shown in Fig. 3. The mass flow rate and the injection velocity of the 39 kg/m^3 ambient density case have been calculated with a 1-D in-house code (Larmi et al., 2002). The differences seen in the shapes of the curves are due to variation in the experimental systems as detailed in Section 4. The boundary conditions for the 115 kg/m^3 ambient gas density case have been calculated with the commercial code GT-Fuel (Keskinen et al., 2012). The mass flow rates and velocities have been calculated at the nozzle exit. In the present study, however, they are applied somewhat downstream from the nozzle exit at $z \sim 6d_n$. It is assumed that within the distance of $6d_n$ ($\sim$2 mm), the liquid volume fraction is high, suggesting only a minor reduction in droplet velocity. Details of the experimental conditions are shown in Table 1. The diesel fuel properties used in the experiments and simulations are presented in Table 2.

As already pointed out, it is assumed that at the nozzle exit there may exist a short intact liquid column. Therefore, modelling of droplets is started a couple of millimetres downstream from the geometrical nozzle hole exit at $z \sim 6d_n$. As a consequence, the flow inside the nozzle as well as the primary breakup process have been omitted. It is clear that these processes have important effects on the subsequent spray formation characteristics in the vicinity of the nozzle. However, as pointed out in several previous studies (Vuorinen et al., 2010a,b, 2011; Martinez et al., 2010), there is a large

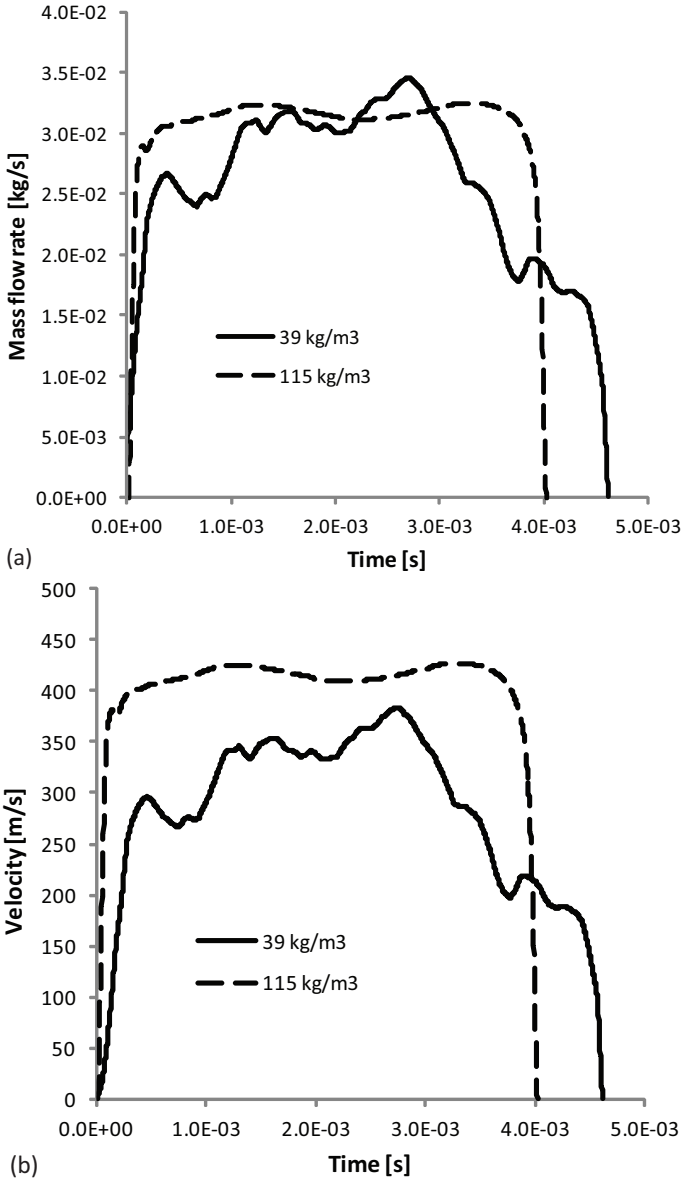

FIG. 3: (a) Simulated mass flow rates; (b) injection velocities in the 39 and 115 kg/m^3 ambient density cases.

TABLE 1: Experimental conditions

Gas density (kg/m^3)	39	115
Nozzle size (mm)	0.37	0.34
Injection pressure (bar)	700	1000

TABLE 2: Fuel properties

Density, +15°C (kg/m^3)	837
Surface tension (N/m)	0.029
Viscosity, +30°C (kg/ms)	0.00269

scale-separation between the near-nozzle scales (say, $<10d_n$) and the global spray properties (say, $50d_n$–$200d_n$), implying that it is possible to model a spray by omitting some of the most complex near-nozzle phenomena.

In the following text we discuss the initial drop size distribution and the associated modelling assumptions at the inlet. The distribution is realized randomly with the box-sampling method using the power-law distribution

$$g\left(d\right) \;=\; \frac{n+1}{n}\left(\frac{d}{d_n}\right)^n \tag{1}$$

In Eq. (1), the exponent n has the value of n = –3.0 in order to yield relatively high probability for small droplets. As a result, the average Sauter mean diameter (SMD) at the droplet origin is about 25 μm. The St numbers at the droplet origin are 82 and 35 in the 39 and 115 kg/m^3 gas density cases, respectively, based on the maximum droplet diameter (assumed $d_n/3$ in the present study).

It is expected that the droplet sizes are generally much smaller at $z \sim 6d_n$ compared to the situation at the nozzle hole exit due to rapid atomization of the liquid. This assumption is based on experimental observations made for example by Hillamo et al. (2010) where the interaction of turbulent flow structures and small droplets could be seen only a few millimeters from the nozzle hole. The requirement for droplets to follow local flow field structures is that the droplet Stokes number $\mathrm{St} = \tau_p/\tau_f$ must be small ($\mathrm{St} \ll 1$). The flow time scale is defined as $\tau_f = L/U$, where L is a characteristic length and U is a characteristic velocity. In the following, it is shown that at $z \sim 6d_n$, there must be a relatively large number of small droplets $d \ll d_n$. According to the St number formula, the condition of $\mathrm{St} \ll 1$ indicates that $d \ll \sqrt{\tau_f 18\nu_g(\rho_g/\rho_d)}$. Therefore, for the given conditions (L = 2 mm, U = 200 m/s, and ρ_g/ρ_d = 0.046), this leads to $d \ll 11$ μm. Consequently, in the present study the maximum droplet diameter a few millimeters from the nozzle hole is restricted to $d_n/3$. At this location, droplets are distributed within a cylindrical volume that has a diameter of $D = 3d_n$ and cylinder height of $z = dz$, where dz is the cell length.

3. GOVERNING EQUATIONS AND NUMERICAL ALGORITHMS

3.1 Fluid Motion

The governing equations for the gaseous phase, describing the conservation of mass, momentum, and energy, are written as

$$\frac{\partial \rho}{\partial t} + \frac{\partial \rho u_j}{\partial x_j} = 0 \tag{2}$$

$$\frac{\partial \rho u_i}{\partial t} + \frac{\partial \rho u_i u_j}{\partial x_j} = -\frac{\partial}{\partial x_j}\left(p\delta_{ij} - \tau_{ij}\right) + M \tag{3}$$

$$\frac{\partial \rho h}{\partial t} + \frac{\partial \rho u_j h}{\partial x_j} = -\frac{\partial}{\partial x_j}\left(\tau_{ij}\, u_j\right) + \frac{\partial}{\partial x_j}\left(\lambda \frac{\partial T}{\partial x_j}\right) \tag{4}$$

where M is the momentum source term exerted from the droplets to the gas phase. The viscous stress tensor is defined as

$$\tau_{ij} = \mu\left(\frac{\partial u_i}{\partial x_j} + \frac{\partial u_j}{\partial x_i}\right) - \mu\frac{2}{3}\frac{\partial u_k}{\partial x_k}\delta_{ij} \tag{5}$$

The Navier–Stokes (NS) Eqs. (2)–(5) are of the form $NS = NS\left(\rho, u_i, ...\right) = 0$ describing the conservation of mass, momentum, and energy. In LES, Eqs. (2)–(5) are spatially filtered resulting in additional subgrid-scale terms from the non-linear part of the equations and they can be written in the form $NS\left(\widetilde{\rho}, \tilde{u}_i, ...\right) = \tau_{sgs}$. The subgrid-scale terms, which need modeling, account for the interaction between the resolved and the unresolved scales. Additionally, according to the Boussinesq hypothesis, viscosity can be written as $\mu = \mu_g + \mu_t$, where μ is the total viscosity and μ_t is the turbulent viscosity calculated from

$$\mu_t = c_1\, \rho \triangle k_{sgs}^{1/2} \tag{6}$$

In Eq. (6), $\triangle$ is the filter width calculated from the cell volume V_{cell} as $\triangle = V_{cell}^{1/3}$. The present study uses a $k - l$ model for the subgrid-scales where a transport equation for the subgrid-scale turbulent kinetic energy k_{sgs} is solved according to

$$\frac{\partial \rho k_{sgs}}{\partial t} + \frac{\partial \rho u_j k_{sgs}}{\partial x_j} = P - \rho\varepsilon_{sgs} + \frac{\partial}{\partial x_j}\left(\mu_t \frac{\partial k_{sgs}}{\partial x_j}\right) \tag{7}$$

where P is the production term calculated as

$$P = \tau_{sgs,\,ij}\,\frac{1}{2}\left(\frac{\partial u_i}{\partial x_j} + \frac{\partial u_j}{\partial x_i}\right) \tag{8}$$

and ε_{sgs} is the subgrid-scale dissipation rate of the turbulent kinetic energy

$$\varepsilon_{sgs} = c_2 \frac{k_{sgs}^{3/2}}{\triangle} \tag{9}$$

The coefficients c_1 and c_2 have the values 0.05 and 1.0, respectively (Hori et al., 2006; Sone and Menon, 2003). The advantage of the present model is that it is capable of capturing non-equilibrium effects between production and dissipation of the kinetic

energy in the sub-grid scales (Sone and Menon, 2003). Additionally, in contrast to an algebraic model (for example the Smagorinsky model), the present model is able to bring the "history" effect to the sub-grid scales (Gibson and Launder, 1978). These factors are especially important in High-Re flows when the simulation is carried out with relatively coarse grid resolution. However, when the resolution of the simulation is fine enough capturing a large portion of the kinetic energy of the turbulent fluctuations, the contribution of the subgrid-scale terms can be considered small. Other option to treat turbulence would be to model turbulence implicitly using the implicit LES approach which has also been used in the context of sprays (Vuorinen et al., 2010a,b) and jets (Vuorinen et al., 2013). A second-order accurate flux limited scheme is used for the spatial discretization and for the time integration a second-order accurate three time level method is used. Simulations have been carried out on a 4-core workstation using the Star-CD 4.16 code.

3.2 Droplet Motion

In LPT, the motion of individual droplets is tracked through the computational domain. As already pointed out, the number of droplets in a diesel spray can be significant and, hence, it may be feasible to group droplets with similar properties into a "parcel." In this study, parcels have equal mass indicating that the number of the droplets within a parcel is varying depending on the droplet size. Furthermore, it is assumed that droplets do not evaporate and there is no interaction between the parcels. The total number of parcels in this study is 435,000.

It is assumed that the force acting on a droplet is due to aerodynamic drag. The droplet equation of motion reads (Crowe et al., 2012)

$$\frac{1}{6}\rho_p \pi d^3 \frac{du_p}{dt} = \frac{1}{2}(u_g - u_p)\,|u_g - u_p|\,\rho_g C_d \frac{\pi d^2}{4} \tag{10}$$

The expression for the drag coefficient C_d is given as

$$C_d = \begin{cases} \dfrac{24}{\mathrm{Re}_p}\left(1 + \dfrac{1}{6}\mathrm{Re}_p^{2/3}\right) & \mathrm{Re}_p < 1000 \\ 0.424 & \mathrm{Re}_p \geq 1000 \end{cases} \tag{11}$$

where Re_p is the droplet Reynolds number based on the droplet slip velocity. The parcel position is updated from

$$\frac{dx_p}{dt} = u_p \tag{12}$$

The droplet velocity change can be calculated from the re-cast form of the Eq. (10) as

$$\frac{du_p}{dt} = \frac{C_d}{\tau_p}\frac{\mathrm{Re}_p}{24}(u_g - u_p) \tag{13}$$

The parcels are advanced in time using a semi-implicit time integration method by taking five subiterations within each time step. The momentum source term M in Eq. (3) is evaluated for each cell separately by looping over all the parcels within the cell. The following relation for the source term is assumed (Crowe et al., 2012)

$$M = \frac{1}{2}\rho_g C_d A \left|u_g - u_p\right| \left(u_g - u_p\right) \frac{1}{V_{cell}} \tag{14}$$

where A is the projected droplet area.

High-resolution LES implies that the subgrid-scale fluctuations are weak and have therefore only minor influence on the droplet motion. If this is not the case, one may add the effects of the subgrid-scale fluctuations in a similar fashion as in the RANS framework, namely, by adding a random velocity vector equal to the local subgrid-scale velocity fluctuation on the droplet velocity. Apte et al. (2003a) have pointed out two aspects regarding the effect of subgrid-scales on the particles: (1) the effect of subgrid-scale modeling is assumed to be important when there is a large amount of kinetic energy in the subgrid scales and when the subgrid-scale time scale is large in comparison to the characteristic droplet time scale, and (2) if a subgrid-scale model is employed, then the particles do feel the effect of the subgrid scales by the resolved scale velocity. There are several LES spray studies where the effect of subgrid-scale fluctuations have been taken explicitly into account (Hori et al., 2006; Oefelein et al., 2007; Bharadwaj and Rutland, 2010) but there are also successful studies without an explicit modeling of the droplet dispersion (Elghobashi, 1991; Eaton and Fessler, 1994; Apte et al., 2003b; Luo et al., 2006; Vuorinen et al., 2010a,b, 2011). Obviously, the approach of not using a separate droplet dispersion model is valid only down to the resolved scales. As pointed out by Apte et al. (2003a), the direct effect of the subgrid scales is expected to be important when the subgrid-scale energy is significant. In their study, they showed the subgrid-scale energy to be close to 10% and concluded that this was small enough for not to use a dispersion model. In the present study, the portion of the subgrid-scale energy will be shown to be close to 5% (see Section 5.5 for details) based on both local and average values. Hence, no explicit modeling of the subgrid-scale fluctuations on droplet dispersion is performed. The consequences of this approach are further discussed in the Results section.

The subgrid-scale contribution on the turbulence produced by droplets may be important under certain circumstances. In the present study, subgrid-scale turbulence production is governed by the velocity gradient of the flow field. The velocity gradient, on the other hand, is mainly produced by the droplet source term in the momentum equation. However, it is possible to take into account the direct production or dissipation of subgrid-scale turbulence due to droplets. This is done by using similar arguments as in the previous discussion of the droplet dispersion modeling. Consequently, direct turbulence production by droplets is important only when the subgrid-scale energy is significant. Hence, in the present modeling approach, we assume that the direct subgrid-scale turbulence production by droplets can be omitted.

3.2.1 Droplet Breakup

The We numbers based on the maximum droplet diameter and the slip velocity at the droplet origin are 7400 and 45,200 in the 39 and 115 kg/m^3 gas density cases, respectively. This implies droplet breakup to be important and, hence, the Wave droplet breakup model is applied (Reitz and Diwakar, 1987). The Wave model gives the rate of change of droplet diameter d as

$$\frac{dd}{dt} = -\frac{(d - d_{stable})}{\tau_b}.$$

According to the regime of breakup, the characteristic breakup time τ_b is calculated for the bag breakup according to

$$\tau_b = \frac{c_{b1}\rho_d^{1/2} d^{3/2}}{4\sigma^{1/2}} \tag{15}$$

and for the stripping breakup as

$$\tau_b = \frac{c_{b2}}{2}\left(\frac{\rho_d}{\rho_g}\right)^{1/2} \frac{d}{|u - u_d|} \tag{16}$$

In order to avoid too rapid droplet breakup, the coefficients c_{b1} and c_{b2} have been given values 20 and 80, respectively, in Eqs. (15)–(16). These values are higher than encountered in typical RANS simulations mainly for two reasons. First, the droplet sizes given close to the nozzle are much smaller than the nozzle diameter as already discussed. For the bag breakup regime in Eq. (15), the characteristic breakup time scale is $\tau_b \sim d^{3/2}$, indicating that if droplet diameter is reduced to $d_n/3$, the resulting time scale is $\sim$1/5 of the original value. For the stripping breakup regime in Eq. (16), the time scale–droplet diameter relationship is linear. Accordingly, if droplet size is to remain at constant values after the breakup process, an increase in the values of the coefficients is needed compared to the situation where much larger droplets are injected. In the (typical) case of the initial droplet size being close to the geometric nozzle hole diameter, there will be no need to change the breakup model coefficients even in context of LES as was observed for example by Kitaguchi et al. (2012). The second reason for the higher coefficient values is that droplet interaction is not taken into account. Typically, droplet interaction modelling increases the average droplet sizes due to coalescence effects.

4. EXPERIMENTS

Experimental fuel spray measurements were carried out with a laser-based backlight imaging system in a pressurized injection test chamber. The details of the methods used in the experiments can be found in Hillamo et al. (2010). In the backlight imaging method, illumination of images is performed with a planar light source. First, a short duration laser pulse is expanded with a lens. While originally green laser light (532 nm)

is shot to a fluorescent plate, the light is phase shifted to white light. This yields even and planar light to the measurements. The light is further smoothed with a milk glass diffuser (Hillamo et al., 2010).

The optical access to the injection test chamber was obtained through four windows at the test chamber walls. The light source was a pulsed Nd:YAG laser sheet with 532 nm wavelength after second harmonic generator. The images were taken with a digital monochrome camera (CCD). The duration of a laser pulse was approximately 5 ns. Due to the short light pulse, the motion of a high-velocity fuel spray is frozen and high timing accuracy can be achieved.

4.1 Experiments at 115 kg/m^3 Gas Density

The test chamber is emulating the physical conditions in diesel engines. However, fuel sprays were non-evaporative (ambient temperature was 20–25°C) and the ambient gas density was kept constant at 115 kg/m^3 by varying the gas pressure which was about 98 bar. According to a general compressibility chart (Nelson and Obert, 1954; Kaario et al., 2010b), it is seen that the deviation from the ideal-gas law is below 3%. The effect of this is considered to be relatively small and it is therefore not taken into account in the present LES/LPT model. The injection pressure was 1000 bar. The maximum variance of injection pressure in the common rail was $\pm$25 bar and the maximum variance of the ambient gas density was $\pm$0.15 kg/m^3. The pressurizing gas, nitrogen (N2), was flowed continuously through the chamber to ensure that the chamber is clear of diesel mist before the next injection. The injector was a solenoid operated common rail injector with a nozzle orifice diameter of 0.34 mm. The angle between symmetrically located orifices was 156 degrees. The images were captured between 0.915 ms and 2.000 ms after electric start of injection. Some delay from the electric injection signal to the fuel jet exit from the nozzle orifice occurred, which was mainly due to solenoid operation, needle inertia, and fluid inertia. Injected fuel was European standard diesel EN590 and the density of the fuel was 837.3 kg/m^3 (15°C). A total of 466 images were taken and analyzed when spray tip penetration was studied. A total of 50 images was taken and analyzed when the spray angle was studied. The experimental procedures are detailed in Hillamo et al. (2008, 2010).

4.2 Experiments at 39 kg/m^3 Gas Density

The experiments conducted for the gas density of 39 kg/m^3 are detailed in Larmi et al. (2002). They were performed in a similar manner as described above. The most significant difference compared to the 115 kg/m^3 high gas density experiments is that in the low gas density measurements also droplet sizes were measured. Larmi et al. (2002) used special cutters to be able to measure droplet sizes from different radial distances from the spray axis at about 60 mm from the nozzle. The droplet sizes were measured

from a fully developed spray after 1 ms from the real start of injection. The spray tip penetration was analyzed using 20–50 images. The spray opening angle was defined using 20 different images. The spray width was defined from a fully developed spray at 62 mm from the nozzle. In addition, a mechanical injection system was used that consisted of a rather long high-pressure pipe between the injector and the pump. This kind of system produces slower pressure rise rates at the injector and higher pressure fluctuations compared to common-rail fuel injection, as is seen in Fig. 3. Tables 1 and 2 summarize the conditions and fuel properties used in the experiments and simulations.

5. RESULTS

5.1 Spray Penetration and Volume

The LES/LPT sprays are shown in Fig. 4 at different times. Droplets are taken from a narrow slice (8 cells thick) to reduce the cluttering of the image by overlapping droplets. There are several important features than can be distinguished from the spray clouds:

1. It takes some time for the spray to become fully turbulent, even though the gas velocity is supplied with random velocity fluctuations at the droplet origin. At earliest times t = 0.6 ms, the onset of the turbulence transition process for the lower gas density spray has only just started, whereas the high gas density spray is already fully turbulent. The faster turbulence transition process is related to the higher Re number of the spray-induced gas jet.

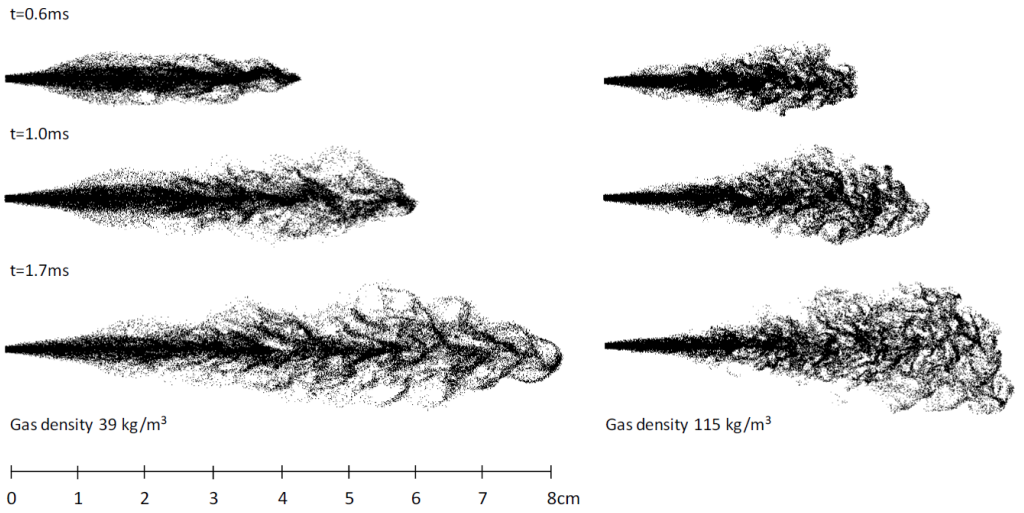

FIG. 4: Fuel sprays with droplets at different times in the 39 kg/m^3 gas density case, left, and in the 115 kg/m^3 gas density case, right. The total injection time is up to 160T or 1.7 ms.

2. It takes some distance from the injector for the spray to become fully turbulent. The high density case exhibits a shorter transition distance. This is again due to the Re number difference of the jets. In addition, the initial St number is high in both cases (St = 82 and 35 in the 39 and 115 kg/m^3 gas density cases, respectively, based on maximum droplet size) indicating that droplets are initially following their trajectories before settling to local flow conditions.

3. Concerning droplet mixing, several important features are visible which can also be seen in experimental sprays. These include local areas with high number density of droplets (preferential concentrations), areas with few droplets (voids free of droplet), and fluctuations (Eaton and Fessler, 1994; Vuorinen et al., 2010a; Hillamo et al., 2010). See also Fig. 7 and the explanations thereafter.

4. The strong effect of the St number to the droplet mixing is clearly visible. The higher density case has a lower St number, implying increased mixing as droplets will follow the local flow structures more effectively. The lower gas density spray has larger areas of preferential concentrations and, additionally, substantial areas of voids, indicating reduced mixing compared to the 115 kg/m^3 density case.

5. The LES/LPT sprays are produced without an explicit dispersion model. Still, several experimental features can be observed (cf. Figs. 4, 6, and 7) and the spray opening angles (cf. Table 3) agree well with the experiments. This suggests that the effect of the subgrid-scales to the droplet trajectories is relatively small.

The spray penetration is an important quantity that influences, for example, the fuel vapor mixing characteristics. The experimental, as well as the predicted spray penetrations, are shown in Fig. 5(a). In the experimental penetration data, each point represents a separate spray realization. The LES/LPT result indicates the cumulative liquid mass up to 98% of the total injected fuel mass. Several features can be characterized from the penetration data. First, initially the higher gas density spray penetrates further than the lower gas density spray. This is contradictory to the known behavior of fuel sprays (Naber and Siebers, 1996). However, this can be explained with the differences in the experimental injection systems, as detailed in Section 4. In addition, the LES/LPT model is capable of capturing the differences in the early spray penetrations between the two gas densities rather well. Second, the spray penetrations at later times have the expected difference that a higher gas density spray penetrates less. Again, the LES/LPT model is able to capture this difference. Thirdly, the LES/LPT predictions of the spray penetrations are in general somewhat overpredicted. The main reason for this is in the boundary condition that is applied at $z \sim 6d_n$, yet it has been originally calculated at $z = 0$.

In addition to the spray penetration, the spray volume evolution is equally important to know, as the volume of the spray plume reveals characteristics of the mean spray air–fuel ratio that can be important for the subsequent combustion process. Assuming a fuel

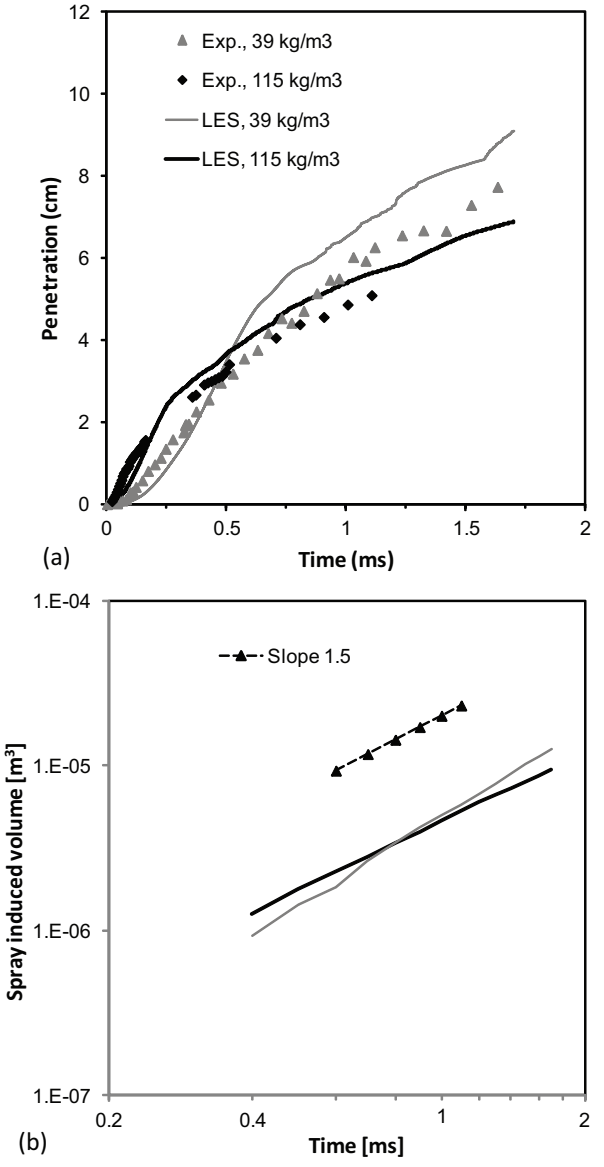

FIG. 5: (a) Experimental and computational spray penetration; (b) spray volume evolution. The total injection time is up to $160T$ or 1.7 ms.

spray volume evolves as a cone–like structure, and using the spray penetration correlation $s \sim t^{1/2}$ (Hiroyasu and Kadota, 1974), it can be shown that the volume evolution of a spray then behaves as $V_s \sim t^{3/2}$ (Vuorinen et al., 2010b). Figure 5(b) shows the comparison of the theoretical spray volume evolution and the predicted spray volume evolution by the LES/LPT model in a log–log plot. The volume of the spray in the LES has

been established by summing up volumes of computational cells where the local velocity magnitude is higher than certain value, in the present study $U_{mag} > 5$ m/s. It was found that this value, although arbitrary, describes the volume of the spray cloud well. Evidently, the volume evolution predicted by the LES/LPT model is in agreement with the theoretical volume development according to $V_s \sim t^{3/2}$. Furthermore, the spray opening angle correlation by Hiroyasu and Kadota (1974) states that $\tan(\alpha/2) \sim (\rho_g/\rho_l)^{1/4}$. Again, assuming the fuel spray to evolve as a cone, the volume evolution of a spray can be shown to obey $V_s \sim \rho_g^{-1/4}\rho_l^{-1/2}$, implying low sensitivity to the ambient gas density. Additionally, it is seen that an increase in gas density decreases the spray volume, a result evident also from Fig. 5(b). This is due to the shorter penetration of the higher density case.

5.2 Spray Shape and Internal Structure

A comparison between LES/LPT and shadowgraph images of diesel sprays in Fig. 6 shows that, although the LES and the shadowgraph images are different in many ways, the general shape of the sprays is well reproduced by LES/LPT. For example, LES/LPT is seen to reproduce the transient and irregular shape of the spray boundary with changing gas density. The internal spray structures in the LES/LPT sprays are compared with particle image velocimetry (PIV) image in Fig. 7. The used PIV system is reported in (Hillamo et al., 2010). The visualization implies that (1) experimentally observed spray structure is highly heterogeneous and characterized by more dense preferential concentrations of droplets, voids, and asymmetric features, (2) the present LES/LPT model shows similar structures implying that the droplet dynamics are well captured without

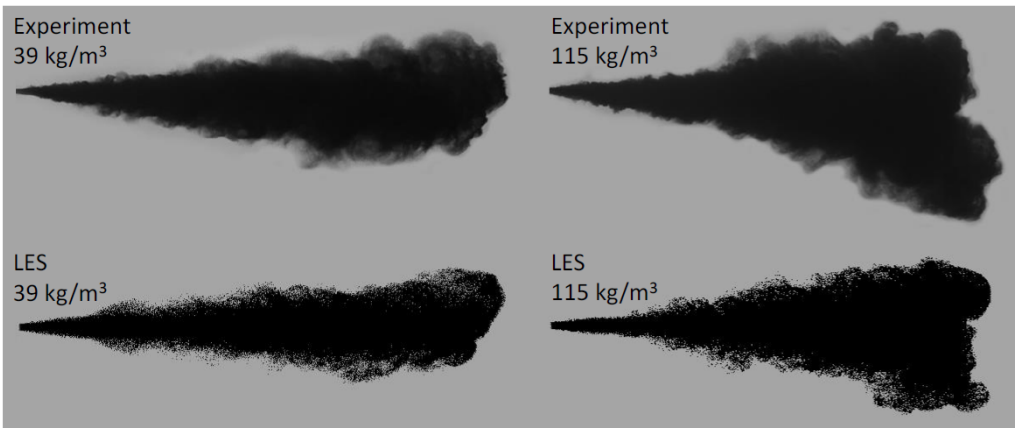

FIG. 6: Qualitative comparison on the spray shapes as obtained with shadowgraphy (top left and top right) and LES (bottom left and right). The lower gas density of 39 kg/m^3 is shown on the left and the higher gas density of 115 kg/m^3 is shown on the right. The tip penetrations are between 50–70 mm.

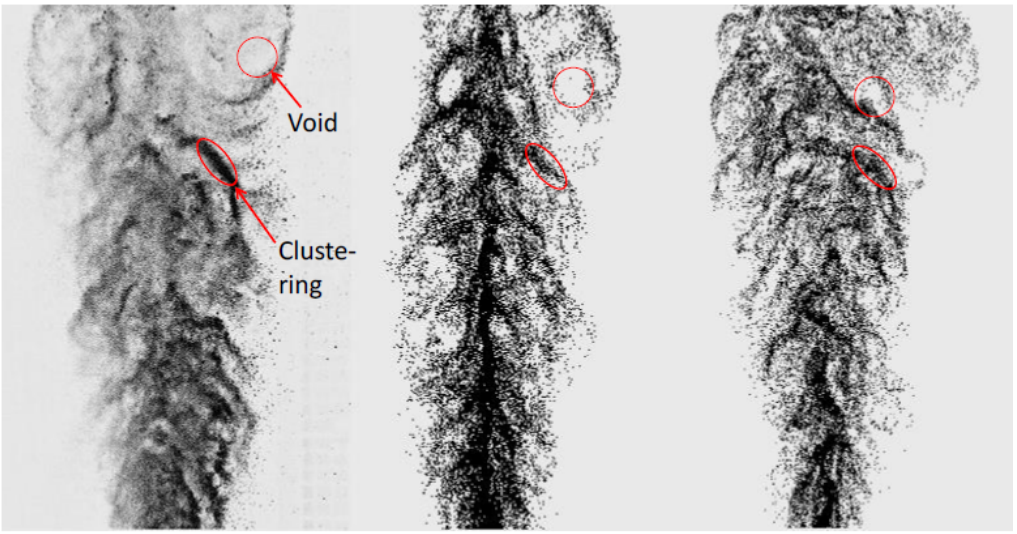

FIG. 7: Qualitative comparison on the random internal structure of sprays and the preferential concentration of droplets. (Left) Experimental PIV measurement. (Middle) LES, gas density is 39 kg/m^3. (Right) LES, gas density is 115 kg/m^3.

an explicit droplet dispersion model, (3) LES/LPT produces certain aspects of the turbulent flow structure, and (4) droplet mixing is seen to be dependent on gas density. In summary, taking into consideration the good correlation between the experimental and the LES/LPT results as discussed above, together with the effects of the LES/LPT subgrid-scale model (detailed in Section 5.5), it is the authors' view that within the present LES/LPT model no separate droplet dispersion model is required. A more detailed discussion on the topic is found in Section 3.2 earlier in this paper.

The depicted spray regions are 20 by 35 mm in size near EOI from the tip region of the sprays. The red circles depict areas with low amount of droplets or voids, and the red ellipses indicate preferential concentrations of droplets.

Spray opening angle is an important parameter in characterizing the overall spray shape. Experimental and computational spray opening angles are shown in Table 3. As expected, higher gas density yields increased spray opening angles. On average, a change in gas density from 39 to 115 kg/m^3 is increasing the whole spray opening angle about

TABLE 3: Experimental and computational spray half opening angle

Gas density (kg/m^3)	39	115
Experimental opening angle (deg)	10.9	12.6
LES opening angle (deg)	11.6	12.6

2.2 degrees. The LES/LPT model is capable of capturing the opening angle with changing gas density very well. The computational results are taken as the average from fully developed sprays in the time interval of 1.0 to 1.7 ms. The opening angle is defined in a similar fashion to the spray penetration, that is, based on the cumulative liquid mass, but in the radial direction. The threshold value used is 99.9%.

Droplet size is a key parameter in fuel sprays affecting the droplet St number and thereby the mixing within the spray. Figure 8 shows the measured SMD at different radial distances from the spray axis in the 39 kg/m^3 density case 60 mm from the nozzle. From the higher gas density case, no droplet size measurements were conducted. The droplet sizes in the experimental and LES/LPT cases have been determined from fully developed sprays ($t > 1$ ms). In the experiments, a cutter technique was used to be able to measure droplet sizes close to the spray axis (Larmi et al., 2002). For the spatial averaging in the LES/LPT, a ring-like volume was defined for each radial distance from the spray axis (the droplet size result was not sensitive to the exact volume used for each radial location). From Fig. 8 it is seen that the droplet sizes are well predicted close to the spray axis. On the other hand, the increasing SMD towards the outer edge of the spray is not captured.

According to the literature (Sangeorzan et al., 1984; Ishikawa et al., 1988; Nakayama, 1988), the cutter technique, which is used to measure the droplet SMD close to the spray axis, affects not only the spray itself but could also affect the measured SMD at the spray axis significantly. Considering the observed droplet SMD at different radial distances

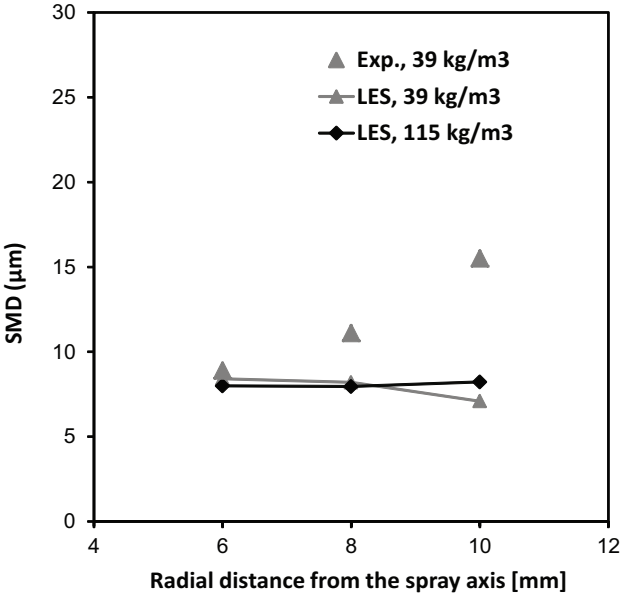

FIG. 8: Experimental and computational spray SMD at different radial distances from the spray axis 60 mm from the nozzle.

from the spray axis in Fig. 8 and taking into account the above mentioned uncertainties in the measurements, the differences seen (experimental droplet SMD between 9 and 15 μm) can be considered to be acceptable. Also, the SMDs of the two gas densities are almost the same, despite the initially higher Weber numbers for the droplets of the higher gas density case. This shows that after a certain distance downstream the SMD is almost independent of the initial Weber number. This behavior can be explained by the fact that, in both gas density cases, initially the droplets are subject to stripping breakup, which leads to small product droplets. Once the droplet Weber numbers are reduced (due to diameter reduction and reduction of the relative drop-gas velocity) they fall into the bag breakup regime and undergo the same breakup mechanism, which according to Eq. (15) is independent of the gas density. Since according to Eq. (16) the stripping breakup depends only on the square root of the gas density, and small droplets have a smaller influence on the SMD, the small differences in the SMDs shown in Fig. 8 are plausible.

5.3 Flow Structures

Small-scale turbulent structures in a flow field can be characterized by the Q-criterion, defined as

$$Q = -\frac{1}{2}\left(S_{ij}S_{ij} - \Omega_{ij}\Omega_{ij}\right) \tag{17}$$

where

$$S_{ij} = \frac{1}{2}\left(\frac{\partial u_i}{\partial x_j} + \frac{\partial u_j}{\partial u_i}\right) \text{ and } \Omega_{ij} = \frac{1}{2}\left(\frac{\partial u_i}{\partial x_j} - \frac{\partial u_j}{\partial u_i}\right)$$

From Eq. (17) it is seen that with positive values of Q, Ω_{ij} must dominate implying mixing and vorticity to be important. On the other hand, with negative values of Q, S_{ij} dominates indicating dissipation and viscosity to be important. A positive Q-criterion showing the small scale turbulent structures where mixing is important is shown in Fig. 9. The color in the Q-isosurface indicates the vorticity in the z-direction, red color indicates clockwise rotation and blue color counterclockwise rotation. The distinct vortex tubes that can be identified in the Fig. 9 are somewhat smaller in diameter in the higher gas density case suggesting finer scale mixing compared to the lower gas density case.

5.4 Mixing Analysis

In the mixing analysis of sprays, the characteristics of droplet mixing are important. However, the St number effects are well established by several previous studies (Luo et al., 2006; Vuorinen et al., 2010a,b, 2011). In addition, in a hot environment the mixing of fuel vapor and air is vital for the combustion process. In the present study, non-evaporative sprays are investigated. In this case, it is perhaps more relevant to investigate

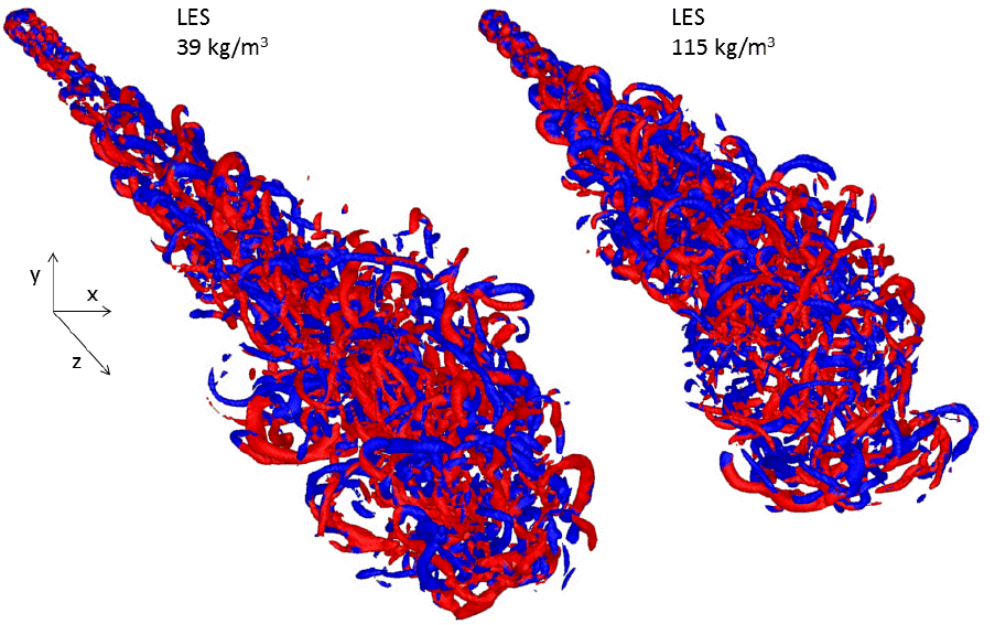

FIG. 9: Q-isosurfaces at time t = 0.9 ms, $Q = 3 \times 10^9$. The positive Q-value used highlights vortex envelopes. (Left) Gas density 39 kg/m^3. (Right) Gas density 115 kg/m^3. The color indicates the vorticity in the z-direction, red color indicates clockwise rotation and blue color counterclockwise rotation.

the air entrainment from the ambient into the spray volume. Here, we propose a new mixing indicator based on studying the mixing of three passive scalars $c_i = c_i\,(x, y, z, t)$, $i = 1, 2, 3$. The main idea of the indicator is to initialize the scalars using the coordinate field values. In particular, the scalars are initialized at $t = 0$ according to $c_1 = x,\ c_2 = y,\ c_3 = z$. This can be clearly understood by looking at the Fig. 10(a) where the initial field is seen as well as the strong movement in the z-direction. The mixing indicator (MI) is defined as

$$MI = \sqrt{(c_1 - x)^2 + (c_2 - y)^2 + (c_3 - z)^2} \tag{18}$$

Thus, MI essentially answers the question: what is the typical distance traveled by a fluid particle at a given time. The MI has units of [MI] = mm. The scalar equation c_i is written as

$$\frac{\partial \rho c_i}{\partial t} + \frac{\partial \rho u_j c_i}{\partial x_j} = \frac{\partial}{\partial x_j}\left(\frac{\mu}{\mathrm{Sc}}\frac{\partial c_i}{\partial x_j}\right) \tag{19}$$

where Sc is the Schmidt number.

Figure 10(a) shows the scalar c_3 evolution and hence the fluid element movement in the axial direction. The scale is in millimeters and it illustrates the distance fluid

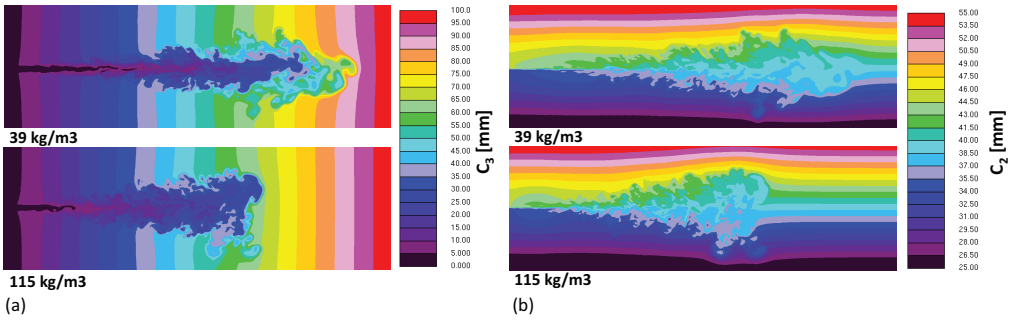

FIG. 10: (a) Scalar c_3 showing fluid element movement from their original position in the axial direction. (b) Scalar c_2 showing fluid element movement from their original position in the radial direction. Situation at t = 1.7 ms. The depicted spray regions are 100 by 30 mm in size.

elements have travelled from their original position. It is seen, for example, that a fluid element which was initially close to the nozzle at z = 5 mm, has traveled to z = 55 mm, a movement of approximately 50 mm. Figure 10(b) shows the scalar c_2 evolution and thereby the fluid element movement in radial direction (y-direction). The coordinate field is zero at the bottom of the mesh and it increases to the maximum value of 80 mm on top of the mesh. Figure 10(b) has been scaled between 25 and 55 mm in order to highlight the radial movement. An air entrainment region is observed extending from the nozzle to roughly halfway between the maximum penetration. Strong radial gas movement is seen in the tip region as well as at the edges of the spray.

Figure 11 shows the calculated mixing indicator MI (taking all directions into account). For example, red color indicates 50 mm fluid element movement from its original

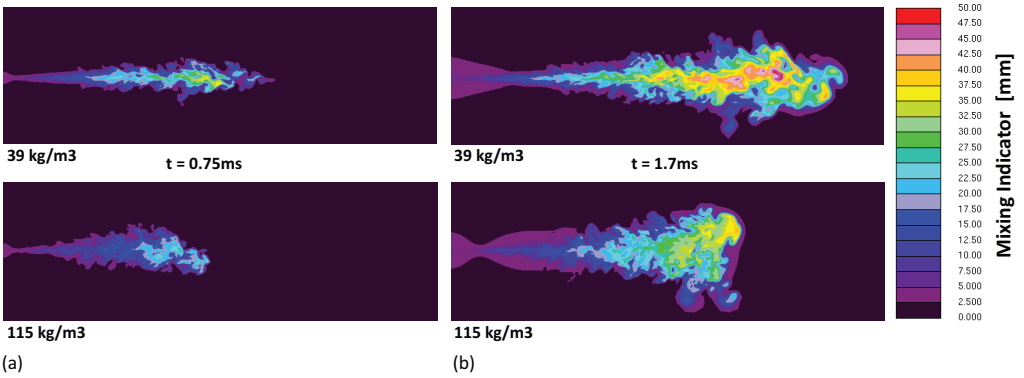

FIG. 11: (a) Gas phase mixing indicator showing fluid element movement in all directions from their original position at t = 0.75 ms. (b) Gas phase mixing indicator at t = 1.7 ms. The depicted spray regions are 100 by 30 mm in size.

position. Furthermore, it becomes clear that areas close to the spray tip are most effectively mixed. It is also seen that the lower gas density case has higher maximum MI values. This is mainly because the lower gas density spray has a higher penetration length at a given time. On the other hand, the situation changes if MI is considered as a function of the spray tip penetration as shown in the Fig. 12(b). In practical applications, such as engines, the spray tip penetration might be a limiting factor due to geometrical

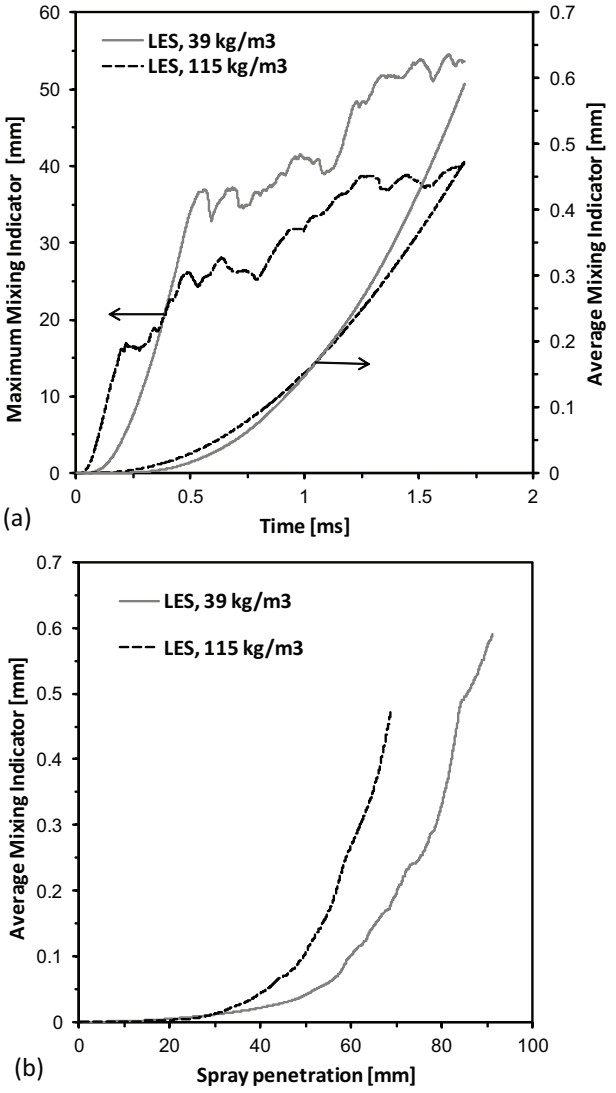

FIG. 12: (a) Average and maximum value of the mixing indicator in the computational domain. (b) Average mixing indicator as a function of spray penetration. Average MI is calculated from the whole computational volume.

constraints. As a consequence, for a given spray penetration, higher gas density is clearly favorable from the gas phase mixing point of view approximately by a factor 2.4.

Finally, it is interesting to discuss the effects of laminar versus turbulent flows on MI. A laminar air stream penetrates in a linear fashion according to $s \sim t\,|\overline{u}|$, where t is time, $\overline{u}$ is the fluid velocity, and s is the penetration length. Accordingly, a laminar air stream would give $MI \sim |\overline{u}|\,t$ (due to linear penetration which can be shown by inserting the change in location $\delta c_1 = x - u_1 t$, and similarly other directions, into the MI equation). However, it is seen from Figs. 12(a) and 12(b) that the average MI is not developing linearly in time. Instead, it grows more rapidly. This suggests turbulence to play an important role on the value of MI. As turbulence is a key factor for a successful mixing to take place in almost any application, it also accelerates the mixing in the present spray system as indicated by the non-linear behavior of the mixing indicator.

5.5 Role of the Subgrid-Scale Model on the Present LES

In order to assess the accuracy of the present LES/LPT model, the portion of the resolved energy is analyzed. Generally speaking, in good quality LES, the portion of the resolved kinetic energy should be high. Estimates given by (Pope, 2001; Celik et al., 2005) indicate that in good quality LES at least 80% of the kinetic energy should be resolved. By definition, the resolved turbulent kinetic energy is calculated from the local velocity as

$$k_{res} = \frac{1}{2}\left(\langle u_i u_i \rangle - \langle u_i \rangle^2\right) \tag{20}$$

where $\langle\ \rangle$ means time averaging over a certain time interval, which is 0.1 ms in the present study. The velocity data has been recorded at two probe points that are located at 53D (59 mm) and 39D (40 mm) from the droplet origin at the spray centerline in the 39 kg/m^3 and 115 kg/m^3 gas density cases, respectively. The magnitude of the subgrid-scale turbulent kinetic energy k_{sgs} is obtained from Eq. (7). The relative portion of k_{sgs} from the total turbulent kinetic energy $k_{sgs} + k_{res}$ is shown in Fig. 13(a). It is seen that both cases yield a relatively similar portion of k_{sgs}. On average, over the whole injection period (considering non-zero points only), the portion of k_{sgs} is 4.6–4.8%. Hence, the resolved portion would be close to 95%. On the other hand, the discretization error of the numerical scheme produces numerical diffusion, which participates to the turbulent diffusion process in a similar fashion as the real diffusion. The numerical diffusion coming from the discretization error can be of the same order of magnitude as predicted by the subgrid-scale model (Pope, 2001). As a result, the resolved portion of the turbulent kinetic energy will be close to 90% in the present study indicating good quality LES. It is well known that numerical methods contain several error sources that influence the simulation result; in particular, the dispersive errors of low order central schemes as well as the diffusive errors of upwind biased schemes influence the results to some extent. In fact, we have recently focused on development of numerical tools for less dissipative turbulence simulations (Vuorinen et al., 2012, 2013).

In order to gain more insight into the LES/LPT model accuracy, in addition to the time averaging described above, also spatial averaging of the velocity data is considered. The volume over which the spatial averaging is performed is based on spray-induced velocity magnitude U_{mag}. A threshold value $U_{mag} > 5$ m/s is used in the present study as it was observed to represent the spray volume evolution accurately. The resulting portion of k_{sgs} is shown in Fig. 13(b). Because of volume definition based on velocity,

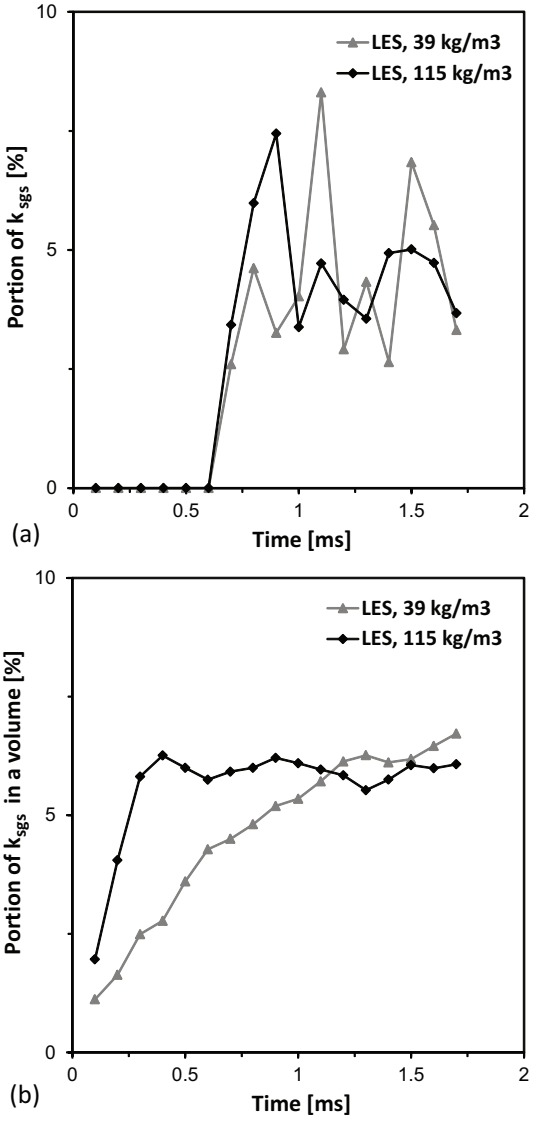

FIG. 13: (a) Portion of the subgrid-scale turbulence from the total turbulence. (b) Portion of the subgrid-scale turbulence inside the spray volume.

the portion of k_{sgs} has non-zero values already at t = 0.1 s and, additionally, the volume averaging process yields a smooth result compared to time averaging only. Furthermore, it is interesting to note that although now a considerably larger volume is considered (compared to only a single computational cell), the resulting portion of k_{sgs} is still close to 5%. Based on the guidelines provided by (Pope, 2001; Celik et al., 2005), this implies good accuracy LES result throughout the spray volume, not only in a single location.

Finally, the present LES/LPT model is compared to a previous study by Kaario et al. (2012) where a coarser mesh was used. A LES quality index (Celik et al., 2005) can be written according to

$$\mathrm{LES}_{IQ} = \frac{1}{1 + [1 - (k_{res}^1 / k_{res}^2)] \, (\alpha^p - 1)^{-1}} \tag{21}$$

where k_{res}^1 and k_{res}^2 are the resolved turbulent kinetic energy in the coarser and denser meshes, respectively (k_{res}^1 = 72.2 and k_{res}^2 = 91.2 in the present study), and $\alpha > 1$ is the grid refinement parameter ($\alpha = 2$), and p is the order of accuracy of the numerical scheme ($p = 2$). The LES quality index aims to characterize the LES/LPT model mainly from the grid resolution point of view. The resulting index is $\mathrm{LES}_{IQ} = 0.935$ implying good mesh resolution. In the discussion by Celik et al. (2005), LES mesh resolution can be considered good if the LES_{IQ} index was above 0.8.

The energy spectra of the radial velocity component are shown in Fig. 14 in the 39 kg/m^3 and 115 kg/m^3 gas density cases, respectively. The velocity data are recorded from the same location as in the case of Eq. (20) between a time interval of 0.6–1.6

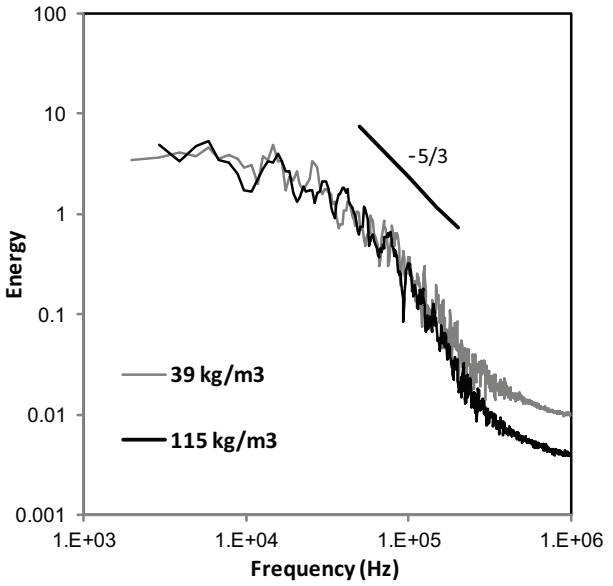

FIG. 14: Energy spectra of the radial velocity component at the spray axis.

ms (39 kg/m^3) and 0.4–1.4 ms (115 kg/m^3). It is seen that there is no accumulation of energy to the higher frequencies, which would imply possible problems in the numerical model. Consequently, the numerical model is dissipative enough. Furthermore, it is seen that the energy cascade process is decaying in a smooth manner, implying that there are no difficulties in the production of small-scale turbulence. Additionally, at higher frequencies, it is seen that there is more energy in the lower gas density case. However, because of the logarithmic scale, the difference in the total amount of energy is very small. It can be attributed to the differences in the boundary conditions and to the fact that the energies are taken from different locations due to the variation of the spray penetration as a function of the gas density.

6. CONCLUSIONS

In the present study fuel spray simulations were carried out using LES/LPT. The spray behavior at two different gas densities was considered, namely a gas density of 39 kg/m^3 and a high gas density of 115 kg/m^3. The objectives of the study were to (1) compare the developed LES/LPT model to previously unpublished experimental data, (2) quantify the effects of ambient gas density variation between 39 and 115 kg/m^3 on fuel sprays, (3) analyze the accuracy of the LES/LPT model by several methods, and (4) develop and apply a novel gas phase mixing indicator to reveal differences in mixing due to gas phase density effects. The following conclusions can be made:

1. The present LES/LPT approach was able to reproduce the experimentally observed global spray characteristics. Gas density had a significant effect on spray penetration, which should be taken into account when designing new engine concepts utilizing gas density values above the typical range.

2. The LES/LPT model produced fuel sprays that resembled experimentally observable local spray structures in many ways. The LES/LPT revealed for example local droplet clustering (preferential concentrations), areas of low concentration of droplets (voids), and significant asymmetry of the sprays.

3. The analysis revealed that the resolved portion of the turbulent kinetic energy was about 95%. Since about 5% of the turbulent energy was in the subgrid scales, their effect on the droplet motion was assumed small and hence no explicit dispersion model was used. Visual inspection of droplet dispersion showed similar trends as seen in experimental sprays. In addition, the predicted spray opening angles were in good agreement with experimental data.

4. The analysis showed that for a given spray tip penetration, higher gas phase mixing was observed approximately by a factor 2.4. In fact, in the present study no negative aspects were found for the higher gas density of 115 kg/m^3 that could affect future engine development.

ACKNOWLEDGMENTS

This research is part of the Future Combustion Engine Power Plant (FCEP) research program. The financial support to the FCEP program from the Finnish Funding Agency for Technology and Innovation, Tekes, is acknowledged. The authors express their gratitude to Harri Hillamo of Aalto University for the experimental figure provided showing internal spray structure.

REFERENCES

Apte, S., Mahesh, K., Moin, P., and Oefelein, J. C., Large-eddy simulation of swirling particle-laden flows in a coaxial-jet combustor, *Int. J. Multiphase Flow*, vol. **29**, pp. 1311–1331, 2003a.

Apte, S., Gorokhovski, M., and Moin, P., LES of atomizing spray with stochastic modeling of secondary breakup, *Int. J. Multiphase Flow*, vol. **29**, pp. 1503–1522, 2003b.

Bharadwaj, N. and Rutland, C., A large-eddy simulation study of sub-grid two-phase interaction in particle-laden flows and diesel engine sprays, *Atomization Sprays*, vol. **20**, no. 8, pp. 673–695, 2010.

Celik, I. B., Cehreli, Z. N., and Yavuz, I., Index of resolution quality for large eddy simulations, *J. Fluids Eng.*, vol. **127**, no. 5, pp. 949–958, 2005.

Chehroudi, B., Chen, S.-H., Bracco, F. V., and Onuma, Y., On the intact core of full-cone sprays, SAE Technical Paper 850126, 1985.

Chesnel, J., Reveillon, J., Mnard, T., and Demoulin, F. X., Large eddy simulation of liquid jet atomization, *Atomization Sprays*, vol. **21**, no. 9, pp. 711–736, 2011.

Crowe, C. T., Schwarzkof, J. D., Sommerfeld, M., and Tsuji, Y., Multiphase Flows with Droplets and Particles, 2nd ed., CRC Press, ISBN 978–1-4398-4050-4, 2012.

Demoulin, F. X., Reveillon, J., Duret, B., Bouali, Z., Desjonqueres, P., and Menard, T., Using direct numerical simulation to improve primary break-up modeling, *Atomization Sprays*, vol. **23**, no. 5, pp. 379–399, 2013.

Eaton, J. and Fessler, J., Preferential concentration of particles by turbulence, *Int. J. Multiphase Flow*, vol. **20**, pp. 169–209, 1994.

Elghobashi, S., On predicting particle-laden turbulent flows, *Appl. Sci. Res.*, vol. **48**, pp. 301–314, 1991.

Elghobashi, S., Particle-laden turbulent flows: Direct simulation and closure models, *Appl. Sci. Res.*, vol. **52**, pp. 309–329, 1994.

Faeth, G. M., Spray combustion phenomena, *Proc. of 26th Symposium on Combustion*, The Combustion Institute, Pittsburgh, pp. 1593–1612, 1996.

Gibson, M. M., and Launder, B. E., Ground effects on pressure fluctuations in the atmospheric boundary layer, *J. Fluid Mech.*, vol. **86**, no. 3, pp. 491–511, 1978.

Gong, Y., Large eddy simulation of dispersed multiphase flow, PhD thesis, Michigan Technological University, USA, 2012.

Hillamo, H., Sarjovaara, T., Kaario, O., Vuorinen, V., and Larmi, M., Diesel spray visualization and shockwaves, *Atomization Sprays*, vol. **20**, no. 3, pp. 177–189, 2010.

Hillamo, H., Sarjovaara, T., Vuorinen, V., Larmi, M., Isaksson, S., and Wik, C., Diesel spray penetration and velocity measurements, SAE Technical Paper 2008-01-2478, 2008.

Hiroyasu, M., and Kadota, T., Fuel droplet size distribution in diesel combustion chamber, SAE Technical Paper 740715, 1974.

Hori, T., Senda, J., Kuge, T., and Fujimoto, H., Large eddy simulation of non-evaporating and evaporative diesel spray in constant volume vessel by use of KIVALES, SAE Technical Paper 2006-01-3334, 2006.

Ishikawa, M., and Murakami, T., Characteristics of intermittent sprays generated by an orifice atomizer, *ICLASS-82*, pp. 75–82, Wisconsin, USA, 1982.

Kaario, O., Imperato, M., Tilli, A., Lehto, K., Ranta, O., Antila, E., Elonheimo, A., Sarjovaara, T., Nuutinen, M., Larmi, M., Rnnskog, T., Pisilä, S., Tiainen, J., Kallio, I., and Rinta-Torala, H., The design of a new generation medium-speed research engine, CIMAC Congress, Paper No. 145, 2010a.

Kaario, O., Nuutinen, M., Lehto, K., and Larmi, M., Real gas effects in high-pressure engine environment, *J. Eng., SAE Int.*, vol. **3**, pp. 546–555, 2010b.

Kaario, O., Hulkkonen, T., Vuorinen, V., Wehrfritz, A., Keskinen, K., and Larmi, M., Numerical and experimental investigation of fuel spray behaviour in very high density environment using LES, *ICLASS*, Heidelberg, 2012.

Kaario O., Larmi M., and Tanner F. X., Non-evaporating liquid spray simulations with the etab and wave droplet breakup models, *ILASS-Europe*, Zaragoza, 2002.

Keskinen, K., Kaario, O., Tilli, A., Hulkkonen, T., and Larmi, M., Improving the accuracy of 1-D fuel injection modeling, SAE Technical Paper 2012-01-1256, 2012.

Kitaguchi, K., Hatori, S., Hori, T., and Senda, J., Optimization of breakup model using LES of diesel spray, *Atomization Sprays*, vol. **22**, no. 1, pp. 57–77, 2012.

Lai, M.-C., Wang, T.-C. T., Xie, X., Han, J.-S., Henein, N., Schwarz, E., and Bryzik, W., Microscopic characterization of diesel sprays at VCO nozzle exit, SAE Technical Paper 982542, 1998.

Larmi, M., Rantanen, P., Tiainen, J., Kiijärvi, J., Tanner, F., and Stalsberg-Zarling, K., Simulation of non-evaporating diesel sprays and verification with experimental data, SAE Technical Paper 2002-01-0946, 2002.

Lemmon, E. W. and Jacobsen, R. T., Viscosity and thermal conductivity equations for nitrogen, oxygen, argon, and air, *Int. J. Thermophys.*, vol. **25**, no. 1, pp. 21–69, 2004.

Luo, K., Klein, M., Fan, J.-R., and Cen, K., Effects on particle dispersion by turbulent transition in a jet, *Phys. Lett. A*, vol. **37**, pp. 345–350, 2006.

Martinez, L., Benkenida, A., and Cuenot, B., A model for the injection boundary conditions in the context of 3D simulation of diesel spray: Methodology and validation, *Fuel*, vol. **89**, pp. 219–228, 2010.

Naber, J. D., and Siebers, D. L., Effects of gas density and vaporization on penetration and dispersion of diesel sprays, SAE Technical Paper 960034, 1996.

Nakayama, M., Developments of a high-resolution and time-resolved particle sizer and its application to intermittent spray sizing, *ICLASS-88*, Sendai, Japan, 1988.

Nelson, L. C. and Obert, E. F., Generalized pvT properties of gases, *Trans. ASME*, vol. **76**, pp. 1057–1066, 1954.

Oefelein, J. C., Sankaran, V., and Drozda, T. G., Large eddy simulation of swirling particle-laden flows in a model axisymmetric combustor, *Proc. Combust. Inst.*, vol. **31**, pp. 2291–2299, 2007.

Parker, T. E., Rainaldi, L. R., and Rawlins, W. T., A comparative study of room-temperature and combusting fuel sprays near the injector tip using infrared laser diagnostics, *Atomization Sprays*, vol. **8**, pp. 565–600, 1998.

Pope, S., *Turbulent Flows, Cambridge University Press*, Cambridge, England, 2001.

Reitz, R. and Diwakar, R., Structure of high-pressure fuel sprays, SAE Technical Paper 870598, 1987.

Sangeorzan, B. P., Uyehara, O. A., and Myers, P. S., Time-resolved drop size measurements in an intermittent high-pressure fuel spray, SAE 841361, 1984.

Smallwood, G. J. and Gülder, Ö. L., Views on the structure of transient sprays, *Atomization Sprays*, vol. **10**, pp. 355–386, 2000.

Sone, K. and Menon, S., Effect of subgrid modeling on the in-cylinder unsteady mixing process in a direct injection engine, *J. Eng. Gas Turb. Power*, vol. **125**, pp. 435–443, 2003.

Stiesch, G., *Modeling Engine Spray and Combustion Processes*, Springer-Verlag, Berlin, 2003.

Vuorinen, V., Hillamo, H., Kaario, O., Larmi, M., and Fuchs, L., Large eddy simulation of droplet Stokes number effects on turbulent spray shape, *Atomization Sprays*, vol. **20**, no. 2, pp. 93–114, 2010a.

Vuorinen, V., Hillamo, H., Kaario, O., Nuutinen, M., Larmi, M., and Fuchs, L., Large eddy simulation of droplet Stokes number effects on mixture quality in fuel sprays, *Atomization Sprays*, vol. **20**, no. 5, pp. 435–451, 2010b.

Vuorinen, V., Hillamo, H., Kaario, O., Nuutinen, M., Larmi, M., and Fuchs, L., Effect of droplet size and atomization on spray formation: A priori study using large-eddy simulation, *Flow Turbulence Combust.*, vol. **86**, no. 3–4, pp. 533–561, 2011.

Vuorinen, V., Larmi, M., Schlatter, P., Fuchs, L., and Boersma, B. J., A low-dissipative, scale-selective discretization scheme for the Navier–Stokes equations, *Comput. Fluids*, vol. **70**, pp. 195–205, 2012.

Vuorinen, V., Yu, J., Tirunagari, S., Kaario, O., Larmi, M., Duwig, C., and Boersma, B. J., Large-eddy simulation of highly underexpanded transient gas jets, *Phys. Fluids*, vol. **25**, no. 1, p. 22, 2013.

Yeh, C.-N., Kosaka, H., and Kamimoto, T., Measurement of drop sizes in unsteady dense sprays, *Recent Advances in Spray Combustion: Spray Atomization and Drop Burning Phenomena*, Summerfield, M. (ed.), AIAA Progress Series, pp. 297–308, 1995.